Structural and Magnetic Characterization of Alternating AB Chains of Composition $[(Cat)_2\{[Mn^{III}(malonate)_2(CH_3OH)_2][Mn^{III}(malonate)_2]\}]_n$ and $[(Cat)_2\{[Mn^{III}(malonate)_2(CH_3OH)][Mn^{III}(malonate)_2]\}]_n$

Salman M. Saadeh,[1] Kathleen L. Trojan,[2,3] Jeff W. Kampf,[1] William E. Hatfield,*[,2] and Vincent L. Pecoraro*[,1]

Departments of Chemistry, The University of Michigan, Ann Arbor, Michigan 48109-1055, and The University of North Carolina, Chapel Hill, North Carolina 27599-3290

Received May 27, 1992

The $S = 2$ chain $[(NH_4^+)_2[Mn^{III}(malonate)_2(CH_3OH)_2][Mn^{III}(malonate)_2]]_n$ (**2**) has been synthesized and structurally characterized by using X-ray diffraction methods. The basic motif of **2** is isostructural to that of the compounds $[K_2[Mn^{III}(malonate)_2(CH_3OH)_2][Mn^{III}(malonate)_2]]_n$ (**1**) and $[(cat)_2[Mn^{III}(salicylate)_2(CH_3OH)_2][Mn^{III}(salicylate)_2]]_n$ (where cat = K^+ (**4**) NH_4^+ (**5**) and Na^+ (**6**)), which have been reported previously. The A-unit includes a six-coordinate Mn^{III} [Mn(1)] with two bidentate malonate ligands occupying the equatorial plane and two methanols bound along an elongated axis. The A-unit is linked to the B-unit through a carboxylate oxygen of the malonate ligand bound to Mn(1). This anti–syn carboxylate bridge occurs on the elongated axis of the B-unit Mn^{III} [Mn(2)]. The equatorial coordination sites of the Mn(2) are filled by two malonate ligands. In addition to providing charge neutrality, the cations constrain the A- and B-units to specific orientations through interactions with the malonate oxygens. A second structure type is observed for $[Na_2[Mn^{III}(malonate)_2(CH_3OH)][Mn^{III}(malonate)_2]]_n$, **3**. Although stoichiometrically identical to the previous chains (i.e., $cat_2Mn_2L_4(CH_3OH)_2$), the complex $[Na_2[Mn^{III}(malonate)_2][Mn^{III}(malonate)_2(CH_3OH)]\cdot(CH_3OH)]_n$ is organized in a dramatically different structure presumably due to a combination of the relatively small malonate moiety and Na^+ radius. The A unit includes six-coordinate Mn^{III} [Mn(1)] with two bidentate malonate ligands (using carboxylate oxygen atoms) occupying the equatorial plane. Both carbonyl oxygen atoms are bound to an adjacent sodium ion [Na(1)]. This leads to a stepped, layer structure with both Mn(1) and Na(1) located on crystallographic inversion centers. The axial ligands to Mn(1) are carbonyl oxygen atoms from malonate ligands with carboxylate oxygen atoms bound to the equatorial positions of the Mn^{III} of the B units [Mn(2) and Mn(2′)]. A second bidentate malonate satisfies the remaining equatorial positions of Mn(2). The Mn(2) is linked to Mn(2′) of the subsequent layer by a carbonyl oxygen atom from the same malonate ligand that is coordinated to Mn(1). The sixth coordination position is filled by a methanol. In every case, there is an anti–syn carboxylate bridge connecting the manganese ions. The magnetic properties of the class of chain typified by **1** can be fit nicely to a modification of the Marathe and Mitra model using the polynomial correction of Hall. The chains are weakly antiferromagnetically coupled with J values in the range -0.09 to -0.18 cm^{-1}, $D \approx -8$ cm^{-1}, and $\langle g \rangle \approx 2.00$ and provide excellent agreement with those parameters reported for the isostructural salicylate chains **4**–**6**. The 3-dimensional lattice was treated using a similar modification of Marathe and Mitra which yielded best fit values of $J_1 \approx -0.24$ cm^{-1}, $D \approx -7.85$ cm^{-1}, and $g \approx 2$. Crystal data for **2**: triclinic, $P\bar{1}$, $a = 8.514(1)$ Å, $b = 8.679(2)$ Å, $c = 9.134(1)$ Å, $\alpha = 95.98(1)°$, $\beta = 112.19(1)°$, $\gamma = 100.27(1)°$, $V = 606.6(2)$ Å^3, $Z = 2$. For 2466 data collected between $5 \le 2\theta \le 50°$ and 2046 data with $I > 0.3\sigma(I)$ the structure refined to $R = 0.043$ ($R_w = 0.062$). Crystal data for **3**: monoclinic, $P2_1/a$, $a = 23.895(4)$ Å, $b = 7.441(1)$ Å, $c = 10.064(2)$ Å, $\beta = 98.04(1)°$, $V = 1772.0(5)$ Å^3, $Z = 3$. For 7331 data collected between $5 \le 2\theta \le 45°$ and 1886 data with $I > 1.5\sigma(I)$ the structure refined to $R = 0.078$ ($R_w = 0.077$).

Introduction

Structural examples of one-dimensional systems containing $S > {}^1/_2$ metal ions are rare[4,5] and explains, in part, why the theory for anisotropic exchange in such systems is not well developed. In particular, there are few linear chain compounds[4,6-8] of manganese(III) that are structurally and magnetically characterized. Interpretation of magnetic susceptibility data is aggravated by the tendency of the single ions to display complicated behavior due to a large number of excited states and zero-field splittings. Often optical or EPR spectroscopies are of limited utility in providing quantitation of zero-field splittings. In particular, X-band EPR studies, in a standard detection mode, often do not detect the Mn^{III} ion as it has relatively rapid electronic relaxation rates and is an $S = 2$ ion often with $D > h\nu$, especially at X-band frequencies.

Single-ion anisotropy is of considerable importance in integer quasi-one-dimensional transition metal complexes. The sign of D determines whether long-range order can occur, since long-range order is precluded by the existence of a singlet ground state. The type of magnetic order is also influenced by the symmetry relations between zero-field split manganese(III) sublattices, and often canting phenomena are found.[6,9,10] A further impetus for studying chain compounds of manganese(III) arises from the Haldane conjecture.[11] Haldane theorized that for certain

(1) The University of Michigan.
(2) The University of North Carolina.
(3) Department of Education Fellow.
(4) Kirk, M. L.; Lah, M. S.; Raptopoulou, C.; Kessissoglou, D. P.; Hatfield, W. E.; Pecoraro, V. L. *Inorg. Chem.* **1991**, *30*, 3900.
(5) Hatfield, W. E.; Eates, W. E.; Marsh, W. E.; Pickens, M. W.; ter Haar, L. W.; Weller, R. W. In *Extended Linear Chain Compounds*; Miller, J. S., Ed.; Plenum Press: New York, 1982; Vol. 3, Chapter 2, p 43.
(6) Kennedy, B. J.; Murray, K. S. *Inorg. Chem.* **1985**, *24*, 1552.
(7) Bonadies, J. A.; Lah, M. S.; Kirk, M. L.; Kessissoglou, D. P.; Hatfield, W.; Pecoraro, V. L. *Inorg. Chem.* **1989**, *27*, 2037.
(8) Day, E. P.; Collins, T. J. Presented at Inorganic Chemistry 91: RACI and NZIC Conference, Hamilton, New Zealand, 1991; Abstract p 2–10.
(9) Kida, J.; Watanabe, T. *J. Phys. Soc. Jpn.* **1973**, *34*, 952.
(10) Gregson, A. K.; Moxon, N. T. *Inorg. Chem.* **1982**, *21*, 586.
(11) Haldane, D. M. *Bull. Am. Phys. Soc.* **1982**, *27*, 181.

0020-1669/93/1332-3034$04.00/0

values of the exchange and single ion anisotropy, a gap opens in the excitation spectrum of the antiferromagnetic integer spin chains and the ground state is a spin singlet. Experimental evidence for a singlet ground state in $S = 1$ chains is limited, and the first example in $S = 2$ chains has recently appeared.[8]

Definition of a variety of isostructural materials containing slight electronic perturbations would be extremely useful in order to achieve a more detailed understanding of these complex systems. In this article, we present structural and magnetic characterization of a series of Mn^{III} chains containing malonate ligands that are isostructural to previously characterized Mn^{III}–salicylate chains. By combining the results of the salicylate and malonate series, we are in a better position to evaluate spin Hamiltonian parameters for one-dimensional, $S = 2$ systems. In addition, we present structural characterization of a unique 3-dimensional system and describe initial attempts to explain its magnetic behavior.

Experimental Section

Materials. Malonic acid, sodium, potassium and ammonium hydroxides, and methanol were purchased from Aldrich Chemical Co. All other chemicals and solvents were reagent grade. Elemental analyses were performed by Galbraith Laboratories, Knoxville, TN, or the Microanalysis Laboratory at the University of Michigan, Ann Arbor, MI.

$[(Cation)_2[Mn^{III}(malonate)_2][Mn^{III}(malonate)_2(CH_3OH)_2]]_n$ (Where Cation = K^+ (1) or NH_4^+ (2). The potassium salt, **1**, was prepared as described previously.[12] The ammonium salt, **2**, was obtained by the reaction of 2.08 g of malonic acid (2 mmol) dissolved in 90 mL of degassed CH_3OH with 2.68 g (10 mmol) of $Mn(AOc)_3 \cdot 2H_2O$. The mixture was stirred for 2 h and then filtered in a glovebag. The supernatant was placed together with a methanolic solution of ammonia into a glovebag and the setup was left in a refrigerator at –20 °C overnight. The mixture was filtered the next morning, and the resultant supernatant was then left under nitrogen for 2–3 days. The green crystalline material used in X-ray studies was recovered by filtration. The overall yield of **1** is 55% and of **2** is 25%. Anal. Calcd for **1**, $K_2Mn_2C_{14}H_{16}O_{18}$ (mol wt 660): C, 25.48; H, 2.44; Mn, 16.65; K, 11.85. Found: C, 25.69; H, 2.42; Mn, 16.81; K, 11.71. Calcd for **2**, $C_{14}H_{24}N_2O_{18}Mn_2$ (mol wt 618): C, 27.21; H, 3.91; N, 4.53; Mn, 17.8. Found: C, 27.08; H, 3.82; N, 4.48; Mn, 17.4.

$[Na_2[Mn^{III}(malonate)_2(CH_3OH)][Mn^{III}(malonate)_2]]_n$ (3). To 0.52 g (5 mmol) of malonic acid dissolved in 25 mL of acetonitrile under nitrogen was added 0.32 g (2 mmol) of $NaMnO_4$. The reaction mixture was stirred for 20–30 min during which time a pale brown solid precipitated and a violet solution remained. Twenty-five milliliters of CH_3OH was added and the mixture stirred until the precipitate dissolved, leaving a pink solution. The solution changed to green after a few hours. Slow evaporation resulted in 0.12 g (38% yield) of pale green crystals of $[Na_2[Mn^{III}(malonate)_2][Mn^{III}(malonate)_2(CH_3OH)] \cdot (CH_3OH)]_n$ (**3**). Anal. Calcd for $Na_2Mn_2C_{14}H_{16}O_{18}$ (mol wt 628.1): C, 26.77; H, 2.57; Mn, 17.49; Na, 7.32. Found: C, 26.88; H, 3.04; Mn, 16.94; Na, 7.01.

Collection and Reduction of X-ray Data. Suitable crystals of **2** and **3** were obtained as described above. The crystals were mounted in glass capillaries. Intensity data were obtained at room temperature for **2** and at 173 K for **3** on a Siemans R3 diffractometer using Mo Kα radiation (0.7107 Å). Three standard reflections were measured every 97 reflections. Modified crystal and data parameters are given in Table I. Intensity data were collected using $\theta/2\theta$ scans. The data were reduced, the structures solved, and the model refined using the Siemans SHELXTL PLUS program package. Computations were carried out on a VAX Station 3500. In the subsequent refinement, the function $\sum w(|F_o| - |F_c|)^2$ was minimized where $|F_o|$ and $|F_c|$ are the observed and calculated structure factor amplitudes. The agreement indices $R = \sum||F_o| - |F_c||/|F_o|$ and $R_w = [\sum w(|F_o| - |F_c|)^2/\sum w|F_o|^2]^{1/2}$ were used to evaluate the results. Atomic scattering factors are from ref 13. For **2**, hydrogen atoms were placed in calculated positions using a riding model $d_{CH} = 0.96$ Å. A common isotopic $U(H)$ was allowed to refine to 0.15(2). For **3**, the methyl hydrogen atoms on C(7) were placed in calculation positions, $d_{CH} = 0.96$ Å, using a riding model. All other hydrogen atoms were located on a difference Fourier map and allowed to refine isotropically. It was necessary to constrain $d_{NH} = 0.85 \pm 0.01$ Å for ammonium hydrogens. A common isotropic $U(H)$ was assigned for all hydrogen atoms and allowed to refine to 0.081(3). Unique data and final R indices are reported in Table I. Fractional atomic coordinates for **1** and **3** are given in Tables II and III, respectively. Selected bond distances and angles for these compounds are provided in Table IV.

Collection and Reduction of Magnetic Data. Magnetic susceptibility data were collected with the use of a Foner-type Princeton Applied Research Model 155 vibrating sample magnetometer. The magnetometer was calibrated with mercury tetrakis(thiocyanato)cobaltate(II).[14] The temperature was mea-

Table I. Summary of Crystallographic Data for $[(NH_4)_2[Mn^{III}(malonate)_2(CH_3OH)_2][Mn^{III}(malonate)_2]]_n$ (**2**) $[Na_2[Mn^{III}(malonate)_2(CH_3OH)_2][Mn^{III}(malonate)_2] \cdot (CH_3OH)]_m$ (**3**)

	3	**2**
formula	$Na_2Mn_2C_{14}H_{16}O_{18}$	$Mn_2C_{14}H_{24}N_2O_{18}$
mol wt	628	618
a, Å	23.895(4)	8.541(1)
b, Å	7.441(1)	8.679(2)
c, Å	10.064(2)	9.134(1)
α, deg	90.00	95.98(1)
β, deg	98.04(1)	112.19(1)
γ, deg	90.00	100.27(1)
V, Å^3	1772.0(5)	606.6(2)
cryst syst	monoclinic	triclinic
space group	$P2_1/a$ (No. 14)	$P\bar{1}$ (No. 2)
Z	3	2
radiation	MoKα (0.7107 Å)	MoKα (0.7107 Å)
temp, K	173	298
R^a	0.0776	0.0425
R_w^b	0.0767	0.0619

$^a R = \sum||F_o| - |F_c||/|F_o|$. $^b R_w = [\sum w(|F_o| - |F_c|)^2/|F_o|^2]^{1/2}$.

Table II. Fractional Atomic Coordinates for $[(NH_4)_2[Mn^{III}(malonate)_2(CH_3OH)_2][Mn^{III}(malonate)_2]]_n$ (**2**)

atom	x	y	z	U_{eq},^{a} Å^2
Mn(1)	0.5	1.0	0.5	0.0253(2)
Mn(2)	0.0	0.5	0.5	0.0253(2)
O(1)	0.6485(2)	0.9849(2)	0.7008(2)	0.0315(7)
O(2)	0.7768(3)	0.8683(3)	0.9075(3)	0.061(1)
O(3)	0.3543(2)	0.7921(2)	0.4696(2)	0.0340(7)
O(4)	0.2843(3)	0.5664(2)	0.5459(3)	0.0397(8)
O(5)	0.0196(2)	0.2853(2)	0.4812(2)	0.0326(7)
O(6)	0.0214(3)	0.0582(2)	0.3530(2)	0.0403(8)
O(7)	–0.0731(3)	0.4895(2)	0.2760(2)	0.0366(8)
O(8)	–0.1785(3)	0.3831(3)	0.0202(2)	0.053(1)
O(9)	0.6644(3)	0.9022(3)	0.3952(2)	0.0428(8)
N(1)	–0.0214(3)	0.2288(2)	0.8359(2)	0.0253(7)
C(1)	0.6764(4)	0.8582(3)	0.7685(3)	0.033(1)
C(2)	0.5832(4)	0.6987(3)	0.6602(4)	0.037(1)
C(3)	0.3942(4)	0.6834(3)	0.5527(3)	0.0285(9)
C(4)	–0.0351(3)	0.1782(3)	0.3514(3)	0.0283(9)
C(5)	–0.1714(4)	0.2030(3)	0.2006(3)	0.037(1)
C(6)	–0.1387(4)	0.3668(3)	0.1592(3)	0.034(1)
C(7)	0.6113(5)	0.7877(4)	0.2536(4)	0.054(1)

$^a U_{eq} = (1/3)\sum_i\sum_j U_{ij} a_i^* a_j^* \mathbf{a}_i \cdot \mathbf{a}_j$.

(12) Lis, T.; Matuszewski, J. *J. Chem. Soc., Dalton Trans.* **1980**, 996.

(13) *The International Tables for X-Ray Crystallography*; Ibers, James A., and Hamilton, Walter C., Eds.; Kynoch Press: Birmingham, England, 1974; Vol. IV, Tables 2.2 and 2.3.1.

(14) Brown, D. B.; Crawford, V. H.; Hall, J. W.; Hatfield, W. E. *J. Phys. Chem.* **1977**, *81*, 1303.

Table III. Fractional Atomic Coordinates for $[Na_2[Mn^{III}(malonate)_2(CH_3OH)][Mn^{III}(malonate)_2]\cdot(CH_3OH)]_n$ (3)

atom	x	y	z	U_{eq},[a] Å^2
Mn(1)	0.0	0.0	0.5	0.0140(6)
Mn(2)	0.19201(5)	0.1966(2)	0.2931(1)	0.0236(5)
Na(1)	0.0	0.5	0.0	0.019(1)
Na(2)	0.0650(1)	0.3950(4)	0.3226(3)	0.029(1)
O(1)	0.0012(2)	0.1534(7)	0.3485(5)	0.016(2)
O(2)	-0.004(2)	0.2192(7)	0.1348(5)	0.023(2)
O(3)	0.0113(2)	-0.2050(7)	0.3956(5)	0.018(2)
O(4)	0.0152(2)	-0.3626(7)	0.2125(5)	0.020(2)
O(5)	0.1337(2)	0.1454(8)	0.3997(5)	0.025(2)
O(6)	0.0938(2)	0.0219(8)	0.5631(5)	0.026(2)
O(7)	0.2463(3)	0.075(1)	0.4141(7)	0.063(3)
O(8)	0.2866(3)	-0.060(1)	0.5940(7)	0.056(3)
O(9)	0.2487(4)	0.2416(8)	0.1847(6)	0.033(2)
O(10)	0.2867(4)	0.380(2)	0.032(1)	0.122(5)
O(11)	0.1366(2)	0.3290(8)	0.1803(5)	0.025(1)
O(12)	0.0960(3)	0.4496(8)	-0.0086(5)	0.029(2)
O(13)	0.1735(3)	-0.0533(9)	0.1867(8)	0.067(3)
O(14)	0.0894(5)	0.535(1)	0.5211(8)	0.108(5)
C(1)	-0.0086(3)	0.111(1)	0.2194(8)	0.015(3)
C(2)	-0.0302(4)	-0.076(1)	0.1847(7)	0.022(3)
C(3)	0.0014(3)	-0.225(1)	0.2677(8)	0.017(3)
C(4)	0.1361(4)	0.064(1)	0.5110(9)	0.028(3)
C(5)	0.1929(6)	0.061(3)	0.601(2)	0.035(6)
C(5A)	0.188(1)	-0.073(4)	0.546(3)	0.04(1)
C(6)	0.2450(4)	0.004(2)	0.527(1)	0.043(4)
C(7)	0.2432(5)	0.320(2)	0.068(1)	0.052(4)
C(8)	0.1876(4)	0.332(2)	-0.012(1)	0.058(5)
C(9)	0.1362(4)	0.373(1)	0.0529(9)	0.027(3)
C(10)	0.1328(8)	-0.170(2)	0.189(2)	0.14(1)
C(11)	0.1122(5)	0.5302)	0.650(1)	0.054(4)

[a] $U_{eq} = (1/3)\sum_i\sum_j U_{ij}a_i^*a_j^*\mathbf{a}_i\cdot\mathbf{a}_j$.

Table IV. Selected Bond Distances (Å) and Angles (deg) for $[K_2[Mn^{III}(malonate)_2(CH_3OH)_2][Mn^{III}(malonate)_2]]_n$ (1) $[(NH_4)_2[Mn^{III}(malonate)_2(CH_3OH)_2][Mn^{III}(malonate)_2]]_n$ (2) and the Average of $[(cat)_2[Mn^{III}(salicylate)_2(CH_3OH)_2]\cdot[Mn^{III}(salicylate)_2]\cdot(CH_3OH)_2(H_2O)_2]_n$ (4–6)

	1[b]	2[c]	4, 5 and 6 (range)[d]
	Bond Distances		
Mn(1)–Cat	3.871(4)	4.049(4)	3.664 (±0.21)
Mn(2)–Cat	3.870(4)	4.104(4)	3.673 (±0.32)
Mn(1)–Mn(2)	5.502(5)	5.510(5)	5.476 (±0.13)
Mn(1)–O(1)	1.918(5)	1.889(2)	1.873 (±0.003)
Mn(1)–O(3)	1.901(4)	1.925(2)	1.925 (±0.001)
Mn(1)–O(9)	2.203(7)	2.207(3)	2.227 (±0.03)
Mn(2)–O(5)	1.901(5)	1.897(2)	1.872 (±0.004)
Mn(2)–O(7)	1.913(5)	1.896(2)	1.922 (±0.004)
Mn(2)–O(4)	2.262(5)	2.247(2)	2.286 (±0.04)
cat–O(8)	2.740(6)		2.608 (±0.26)
cat–O(4)	2.676(6)		2.686 (±0.20)
cat–O(3)	2.802(5)	3.104(4)	2.703 (±0.19)
cat–O(1)	2.904(5)		2.689 (±0.26)
cat–O(5)	2.714(5)		2.676 (±0.26)
cat–O(6)	2.796(6)	2.883(4)	2.813 (±0.28)
cat–O(2)		2.815(4)	
cat–O(7)		2.850(4)	
	Bond Angles		
O(1)–Mn(1)–O(2)	92.1(2)	91.6(1)	93.1 (±0.8)
O(1)–Mn(1)–O(9)	88.8(2)	91.9(1)	88.8 (±0.7)
O(2)–Mn(1)–O(9)	87.9(2)	92.5(1)	88.6 (±1.1)
O(3)–Mn(2)–O(5)	91.2(2)	84.6(1)	96.2 (±0.6)
O(3)–Mn(2)–O(6)	93.6(2)	92.9(1)	91.0 (±1.0)
O(5)–Mn(2)–O(6)	91.5(2)	91.5(1)	92.2 (±0.6)

[a] Oxygens with asterisks denote atoms from adjacent chain (chain 2). Printed atoms are symmetry-related first coordination sphere oxygen atoms. [b] Bold separations are contacts associated with weak hydrogen bonds. [c] From ref 12. [d] The numbering scheme for chains **4**, **5**, and **6** used in ref 4 differs from that of chains **1** and **2** since the latter molecules have additional oxygen atoms. The chemically equivalent distances are compared in this table.

sured with a gallium arsenide diode, which had been standardized against a calibrated diode. Diamagnetic corrections for the constituent atoms were made by using Pascal's constants.[15] Samples containing approximately 150 mg of finely powdered compound were contained in precision-milled Lucite sample holders. The magnetic susceptibility was measured in a field of 10 kOe. A Simplex[16] nonlinear least-squares fitting procedure was used in the analysis of the experimental magnetic susceptibility data. The best fit criterion was the minimum of the function $F = \sum (\chi_i^{obsd}T - \chi_i^{calcd}T)^2/(\chi_i^{obsd}T)^2$.

Results

Structural Description of AB-Type Chains. The solid-state structures of two manganese^{III} AB-type chain complexes of chemical formula $[(NH_4)_2[Mn^{III}(malonate)_2(CH_3OH)_2][Mn^{III}(malonate)_2]]_n$ (**2**) and $[Na_2[Mn^{III}(malonate)_2][Mn^{III}(malonate)_2(CH_3OH)]\cdot(CH_3OH)]_n$ (**3**) have been determined. An ORTEP[17] diagram of **2**, which is isostructural with the K^+ salt previously reported[12] (**1**) showing the Mn(1) and Mn(2) polyhedra are provided as Figures 1 and 2, respectively. ORTEP diagrams of **3** showing the Mn(1), Mn(2) polyhedra are shown as Figures 3 and 4, respectively. The connectivity between Mn(1) and Mn(2) is shown by Figure 5, the connectivity between Mn(2) atoms is shown by Figure 6, and a view of the extended area, looking down the crystallographic *b* axis is provided as Figure 7.

$\{(cat)_2[Mn^{III}(malonate)_2(CH_3OH)_2][Mn^{III}(malonate)_2]\}_n$ salts. The basic chain motif is isostructural with a series of $\{(cat)_2[Mn^{III}(salicylate)_2(CH_3OH)_2][Mn^{III}(salicylate)_2]\}_n$ salts, where cat = K^+ (**4**), NH_4^+ (**5**), and Na^+ (**6**), that we have previously examined.[4] Important bond lengths and angles for **1**, **2**, and the average of **4**, **5**, and **6** are provided for comparison in Table IV. Compound **1** crystallizes in the triclinic space group, $P\bar{1}$, with both Mn(1) and Mn(2) located on crystallographic inversion centers. The resultant molecular structure is composed of three parts: (i) the polyhedron of Mn(1) in $Mn^{III}(malonate)_2(CH_3OH)_2$ (the A unit); (ii) the polyhedron of Mn(2) in $Mn^{III}(malonate)_2$ (the B unit) which is bridged to the A structure by two carboxylates; (iii) the monovalent cation coordination environment. An abbreviated structural description is given since detailed discussions are available for **1**, **4**, **5**, and **6**.

Manganese Polyhedra. The Mn(1) polyhedron is six-coordinate by virtue of two bidentate malonate ligands that form a tetragonal plane and two axial solvent methanols. The in-plane carboxylate oxygens atoms are at relatively short average distances of 1.91(1) Å. There is little variation across the five compounds (malonates and salicylates) so far examined. As shown in Table IV, the coordinated methanol oxygens reside at longer distances (≥2.26 Å). Such marked axial elongations are typical for high-spin d^4 systems. The most sensitive Mn–O bond to cation and/or ligand substitution is along the Jahn–Teller axis. This observation provides information about the microscopic orientation of electron density in the unit and, as discussed more fully below, is consistent with an energy diagram which places the unoccupied $d_{x^2-y^2}$ orbital at highest energy. Despite the axial elongation, all of the O–Mn–O bond angles are within 3° of the predicted octahedral value.

The Mn(2) ion is also six-coordinate. The four equatorial sites are filled with oxygen atoms [O(5), O(7), O(5b), O(7a)] from bidentate malonate ligands, while the axial ligands of this metal are carboxylate oxygens [O(4) and O(4a)] from the malonates of the A unit. This leads to an anti–syn AB-type chain. Once again, the two bidentate malonate groups form the basis for the *xy* plane with short Mn–O distances that are shown

(15) (a) Figgis, B. N.; Lewis, J. In *Modern Coordination Chemistry*; Lewis, J., Wilkins, R. G., Eds.; Interscience: New York, 1960; Chapter 6, p 403. (b) Konig, E. *Magnetic Properties of Transition Metal Compounds*; Springer-Verlag: West Berlin, 1966. (c) Weller, R. R.; Hatfield, W. E. *J. Chem. Educ.* **1979**, *56*, 652.
(16) Nelder, J. A.; Mead, R. *Comput. J.* **1965**, *7*, 308.
(17) Johnson, C. K. ORTEP-II: A FORTRAN Thermal-Ellipsoid Plot Program for Crystal Structure Illustrations. Report ORNL-5138; Oak Ridge National Laboratory: Oak Ridge, TN, 1976.

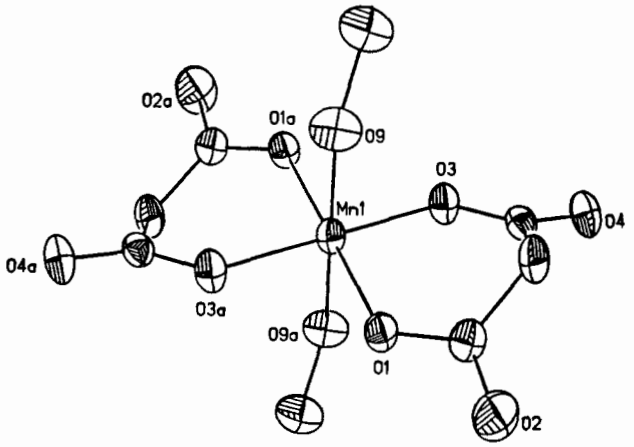

Figure 1. ORTEP diagram of the Mn(1) polyhedron of **2** with thermal ellipsoids at 50% probability.

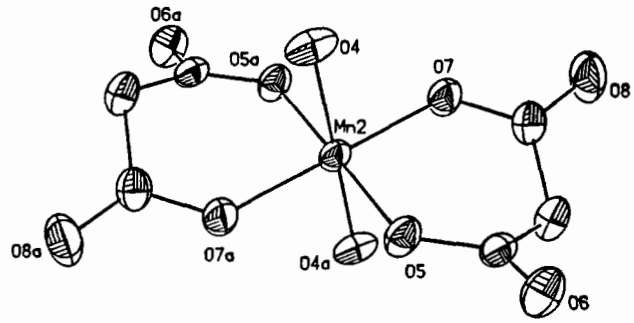

Figure 2. ORTEP diagram of the Mn(2) polyhedron of **2** with thermal ellipsoids at 50% probability.

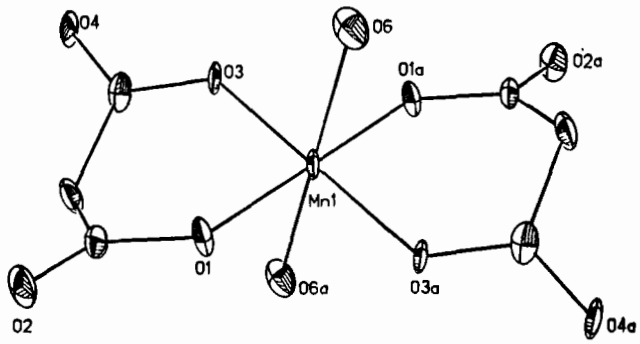

Figure 3. ORTEP diagram of the Mn(1) polyhedron of **3** with thermal ellipsoids at 50% probability.

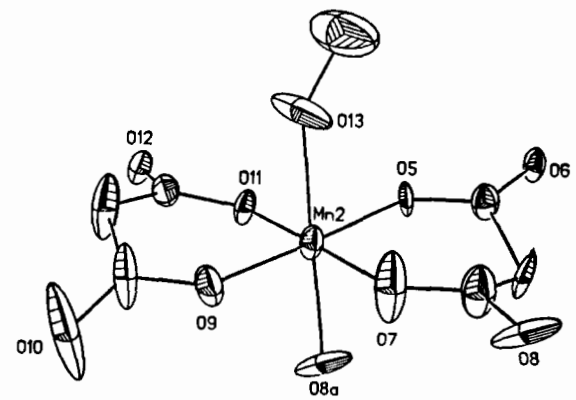

Figure 4. ORTEP diagram of the Mn(2) polyhedron of **3** with thermal ellipsoids at 50% probability.

in Table IV to be indistinguishable from the A unit and are relatively insensitive to cation substitution. The axial carboxylates of Mn(2) show even greater tendency to elongate than the methanols on Mn(1) (e.g., 2.21 Å vs 2.25 Å). Furthermore, the

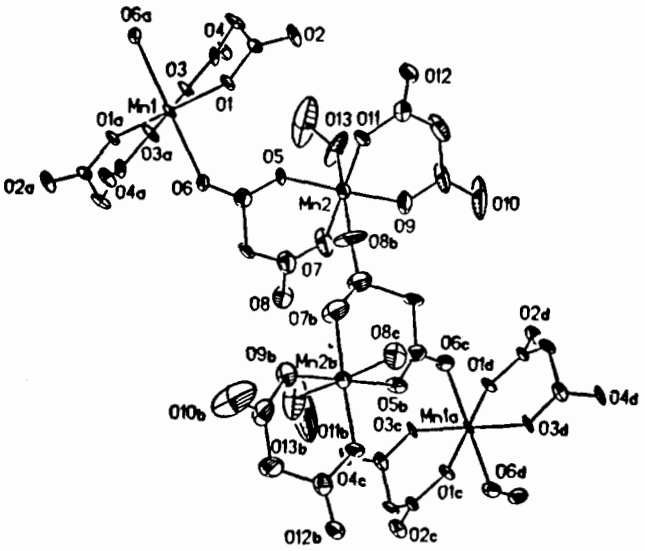

Figure 5. ORTEP diagram of the Mn(1) and Mn(2) polyhedra of **3** with thermal ellipsoids at 50% probability and illustrating carboxylate bridges that link Mn(1) to Mn(2) and Mn(1) to Mn(1b).

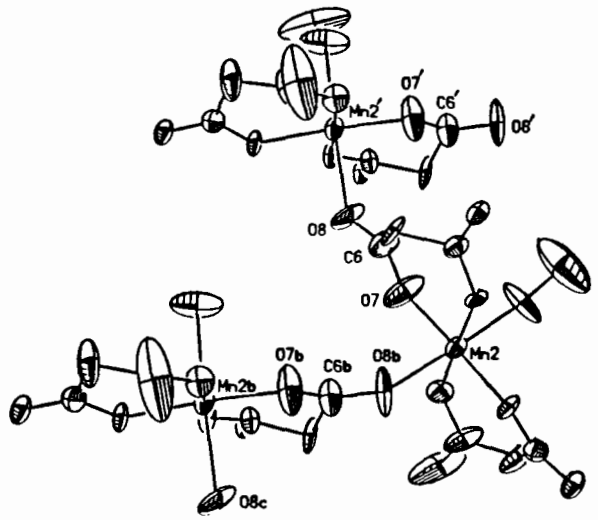

Figure 6. ORTEP diagram of the Mn(2) and Mn(2b) polyhedra of **3** with thermal ellipsoids at 50% probability and illustrating syn–anti carboxylate bridges that link Mn(2) to Mn(2b).

average and individual Mn(2)–O(4) distances are consistently longer than those seen for Mn(1)–O(9) for the respective salts, although the same trend on axial bond length elongation is observed. This suggests that the lowest energy d_{z^2} orbital in all of these complexes resides on Mn(2) in **2**.

Neither the Mn(1) nor the Mn(2) polyhedra are markedly different from the related salicylate chains; however, it can be seen that the coordination spheres of Mn(1) and Mn(2) in the malonate chains are more symmetric. For example, comparison of the O(1)–Mn(1)–O(2) and O(5)–Mn(2)–O(6) angles for the K^+ chains **1** and **4** give 92.1 vs 93.9° and 91.5 vs 92.8°, respectively. This is likely due to the shorter Mn–O(phenolate) vs Mn–O(carboxylate) bonds (average = 1.875 Å in **4** vs 1.901 Å in **1**) that tend to twist the salicylate oxygen atoms closer to the manganese.

Cation Polyhedra. Charge balance is achieved by the incorporation of two monovalent cations which are associated with each AB unit. The potassium cation is six-coordinate, giving contacts with six oxygen atoms from two chains. A better description for the ammonium cation is that it forms hydrogen bonds to malonate oxygens O(2), O(3), O(6), and O(7).

$[Na_2[Mn^{III}(malonate)_2[Mn^{III}(malonate)_2(CH_3OH)]\cdot(CH_3OH)]_n$ (3). A slight variation of the crystallization conditions

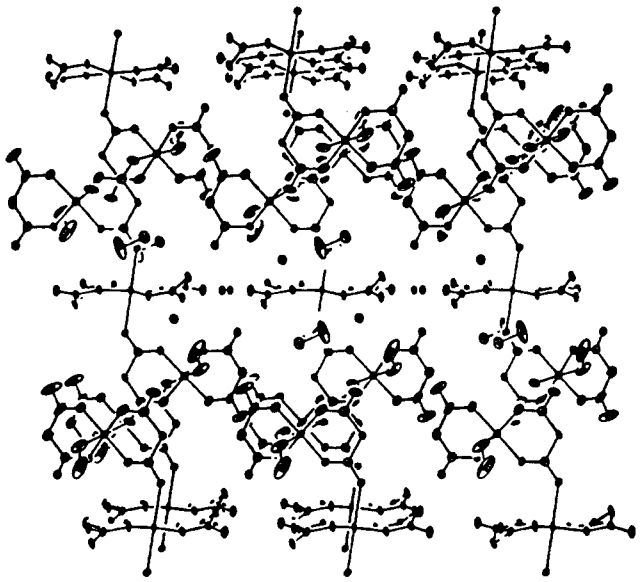

Figure 7. ORTEP diagram of 3 illustrating the interconnectivity between manganese ions of the chains. Bonds to sodium ions have been omitted for clarity.

Table V. Selected Distances (Å) and Angles (deg) for $[Na_2[Mn^{III}(malonate)_2(CH_3OH)_2][Mn^{III}(malonate)_2]\cdot(CH_3OH)]_n$ (3)

	Bond Distances[a]		
Mn(1)–Na(1)	6.259(3)	Mn(1)–Na(2)	3.875(4)
Mn(2)–Na(1)	5.574(3)	Mn(2)–Na(2)	3.427(4)
Mn(1)–Mn(2)	5.497(2)	Mn(2)–Mn(2a)	5.970(2)
Mn(1)–O(1)	1.908(4)	Mn(1)–O(3)	1.893(5)
Mn(1)–O(6)	2.248(5)	Mn(2)–O(5)	1.912(5)
Mn(2)–O(7)	1.883(7)	Mn(2)–O(8a)	2.161(7)
Mn(2)–O(9)	1.885(6)	Mn(2)–O(1)	1.894(5)
Mn(2)–O(13)	2.161(7)		
Na(1)–O(2)	2.493(5)	Na(1)–O(4a)	2.353(5)
Na(1)–O(12)	2.339(6)	Na(2)–O(2)	2.27(6)
Na(2)–O(2)	2.627(6)	Na(2)–O(5)	2.530(5)
Na(2)–O(11)	2.432(6)	Na(2)–O(14)	2.256(8)
	Bond Angles		
O(1)–Mn(1)–O(3)	91.1(2)	O(1)–Mn(1)–O(3a)	88.9(2)
O(1)–Mn(1)–O(6)	93.2(2)	O(1)–Mn(1)–O(6a)	86.8(2)
O(3a)–Mn(1)–O(6)	89.9(2)	O(3a)–Mn(1)–O(6a)	90.1(2)
O(5)–Mn(2)–O(7)	91.8(3)	O(5)–Mn(2)–O(8a)	90.6(2)
O(5)–Mn(2)–O(9)	178.3(3)	O(5)–Mn(2)–O(11)	86.4(2)
O(5)–Mn(2)–O(13)	89.5(3)	O(8a)–Mn(2)–O(9)	91.1(2)
O(8a)–Mn(2)–O(11)	88.5(2)	O(8a)–Mn(2)–O(13)	177.4(3)
O(9)–Mn(2)–O(11)	93.4(2)	O(9)–Mn(2)–O(13)	88.8(2)
O(11)–Mn(2)–O(13)	94.2(2)		

reproducibly produces a three-dimensional motif that is very different from that seen in **1**, **2**, and **4**–**6**. Compound **3** crystallizes in the monoclinic space group $P2_1/a$, with both Mn(1) and Na(1) located on crystallographic inversion centers. The second manganese and second sodium ions are located on general positions. The resultant molecular structure is composed of four parts: (i) the polyhedron of Mn(1) in $Mn^{III}(malonate)_2$ (the A unit); (ii) the polyhedron of Mn(2) in $Mn^{III}(malonate)_2(CH_3OH)$ (the B unit), which is bridged to the A structure by a carboxylate oxygen and to a B′ unit by a carbonyl oxygen; (iii) the Na(1) coordination sphere, with six oxygen atoms arising from malonate oxygens, that leads to sheets composed of alternating Mn(1) positions; (iv) the Na(2) coordination sphere, which stabilizes the chain and sheet structure. Important bond lengths and angles for this structure are provided in Table V. In the discussion of Figures 5–8, Mn(2) and Mn(2a) are symmetry related through Mn(1), which is located on a crystallographic inversion center. The atoms Mn(2b) and Mn(2a) are chemically equivalent and are related by a translation to the Mn(1) of the next layer. The designation Mn(1′) corresponds to a translation

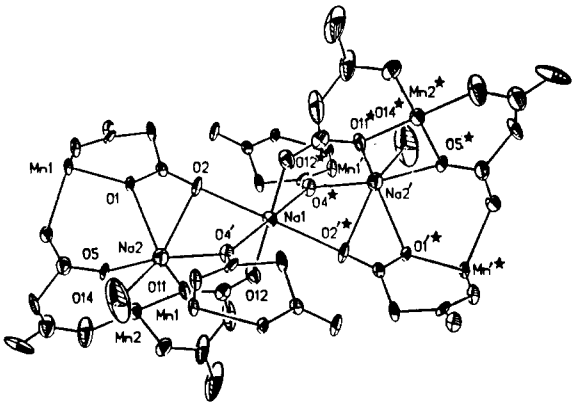

Figure 8. ORTEP diagram of 3 illustrating Na(1) and Na(2) polyhedra.

of Mn(1) within a specific $Na[Mn^{III}(malonate)_2]$ layer while Mn(1*) specifies a translation to a Mn atom in the next layer (i.e., a translation perpendicular to that of Mn(1)–Mn(1′)).

Manganese Polyhedra in 3. As shown in Figure 3, the Mn(1) ion is six-coordinate by virtue of carboxylate oxygen atoms from two bidentate malonate ligands [O(1), O(3), O(1a), and O(3a)] that form the tetragonal plane, and two oxygen atoms [O(6) and O(6a)] from malonate ligands bound in the polyhedra of Mn(2) and Mn(2a). The in-plane carboxylate oxygens are at relatively short average distances that are comparable to the bond lengths observed for complexes **1** and **2** above. The Jahn–Teller axis is oriented along the O(6)–Mn(1)–O(6a) vector with marked elongations reported in Table V that are typical for high-spin d^4 systems. Despite the axial elongation, all of the O–Mn–O bond angles are within 5° of the predicted octahedal value. Oxygen atoms from the malonates in the tetragonal plane of Mn1 [O(2), O(4), O(2′), and O(4′)] are ligands to Na(1). The structural ramifications of this donation will be described more fully below.

The Mn(2) polyhedron, shown as Figure 4, is six-coordinate with five of its sites filled with malonate oxygen atoms and the sixth position occupied by methanol, O(13). Two bidentate malonates span the equatorial positions [O(5), O(7); O(9), O(11)] at typical Mn^{III}–O(carboxylate) distances given in Table V. The fifth malonate derived oxygen, O(8a), comes from one of the malonate moieties bound equatorially to Mn(2a). The axial carboxylate and methanol of Mn(2) show the expected Jahn–Teller elongation. Once again the angles of the manganese polyhedron are close to the predicted octahedral values.

The Mn(1) and Mn(2) atoms are linked in a three-dimensional structure by two interpenetrating chain motifs. The first connectivity pattern given as $[Mn(2b)–Mn(1)–Mn(2)–Mn(2a)–Mn(1a)–Mn(2c)]_n$ units can be traced through atoms Mn(1)–O(6)–C(4)–O(5)–Mn(2)–O(8a)–C(6a)–O(7a)–Mn(2a)–O(5a)–C(4a)–O(6a)–Mn(1a)– *etc.* This yields an ABBA-type chain that is illustrated in Figure 5. The malonate linker region O(6)–C(4)–O(5) spans from the d_{z^2} orbital of Mn1 to the $d_{x^2-y^2}$ orbital of Mn(2). Similarly, the malonate linker region O(8a)–C(6a)–O(7a) spans from the d_{z^2}-orbital of Mn(2) to the $d_{x^2-y^2}$ orbital of Mn(2a). Notice that the same malonate that links Mn(1a) to Mn(2a) also links Mn(2) to Mn(2a). The second chain motif is illustrated in Figure 6. The connectivity pattern is given as $[Mn(2b)–Mn(2)–Mn(2a)]_n$ units and can be traced through atoms Mn(2b)–O(8)–C(6)–O(7)–Mn(2)–O(8a)–C(6a)–O(7a)–Mn(2a)– *etc.* As described above, the malonate linker region O(8)–C(6)–O(7) spans from the d_{z^2} orbital of Mn(2) to the $d_{x^2-y^2}$ orbital of Mn(2c).

The two chain motifs form a junction at Mn(2) that leads to a three-dimensional connectivity pattern for the Mn(III) ions that is shown in Figure 7. Propagation of the first chain motif is in the plane of the page in a nearly horizontal direction (*a* axis). The second chain zigzags out of the page toward the observer along the crystallographic *b* axis. The three-dimensional character

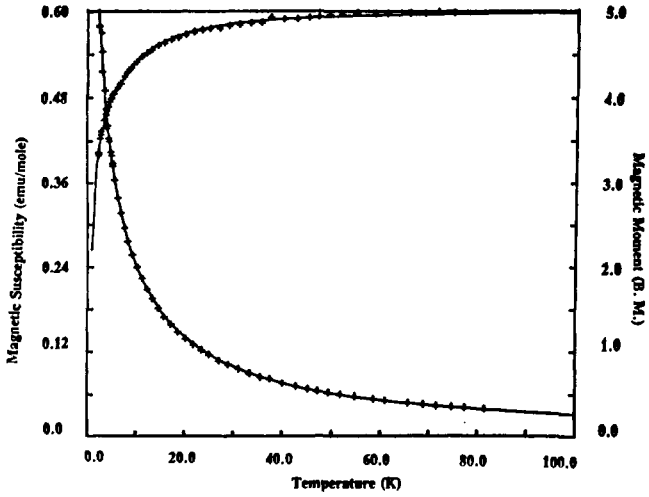

Figure 9. Temperature dependent magnetic susceptibility of **1** in a magnetic field of 10 kOe. The best fit parameters obtained are $J = -0.18$ cm^{-1}, $D = -7.85$ cm^{-1}, and $zJ' = 0$ cm^{-1} with $g_{\parallel} = 1.99$ and $g_{\perp} = 1.98$. The best fits calculated for both χ vs T and μ vs T are illustrated as solid lines.

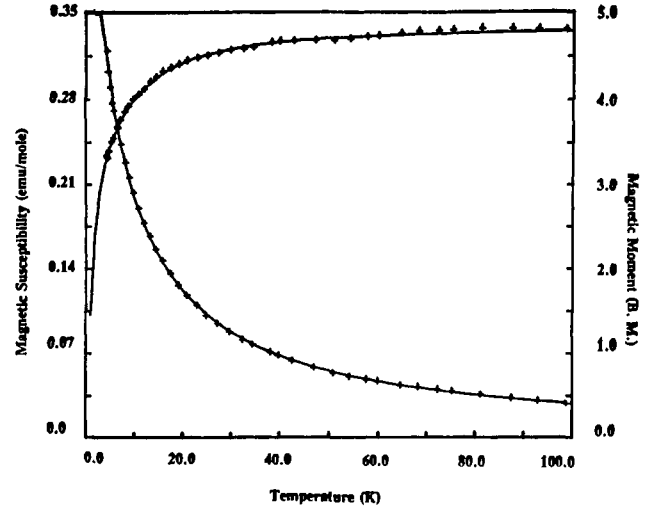

Figure 10. Temperature dependent magnetic susceptibility of **2** in a magnetic field of 10 kOe. The best fit parameters obtained are $J = -0.09$ cm^{-1}, $D = -7.55$ cm^{-1}, and $zJ' = 0$ cm^{-1} with $g_{\parallel} = 2.09$ and $g_{\perp} = 2.03$. The best fits calculated for both χ vs T and μ vs T are illustrated as solid lines.

of the system is completed along the c axis by alternating Mn and Na ions located on crystallographic inversion centers.

Sodium Polyhedra. Charge balance is achieved by the incorporation of two monovalent cations, one of which is located on a crystallographic inversion center [Na(1)] and the other [Na(2)] is found on a general position. The sodium cations are both six-coordinate as shown in Figure 8. Four of the six oxygens [O(2), O(4), O(2′), and O(4′)] coordinated to Na(1) are from malonate ligands that are also coordinated to four independent Mn(1) atoms. Thus, the Mn^{III}(malonate)$_2$ planes are tethered together into a three-dimensional array via this sodium atom as depicted in Figure 8. These planes are viewed edge on in the center of the Figure 7 diagram running from top to bottom. The remaining axial coordination sites are filled by oxygen atoms O(12) and O(12a) from malonate ligands that are bound to Mn(2) and Mn(2a). The Na(2) polyhedron is also six-coordinate, as illustrated in Figure 8, with five malonate oxygen atoms and a coordinated methanol. Three oxygen atoms (O(1), O(2), O(4)) come from two malonates that are bound to Mn(1) and Mn(1*). Two oxygens (O(5) and O(11)) come from two malonates bound to Mn(2′).

Analysis of Magnetic Susceptibility Data. The details of the analysis of magnetic susceptibility data for Mn^{III} $S = 2$ chains were given earlier.[4] Essentially, it was assumed that the spin-Hamiltonian parameters, D, $g_{1'}$, and g_1 for each manganese ion were the same for the manganese ions in the two sites along the chain and that E was negligible.

Magnetic susceptibility of [K$_2$[Mn^{III}(malonate)$_2$(CH$_3$OH)$_2$]-[Mn^{III}(malonate)$_2$]]$_n$ (1). The temperature-dependent magnetic susceptibility of [K$_2$[Mn^{III}(malonate)$_2$(CH$_3$OH)$_2$][Mn^{III}(malonate)$_2$]]$_n$ in a magnetic field of 10 kOe is shown in Figure 9. Isothermal magnetization data as a function field strength were obtained between 50 and 15 kOe at 4.17 K and were obtained over this range of field strengths. Since the susceptibility does not turn over at the lowest temperatures studied, it is assumed that the intrachain interactions are small and that the chain may be treated by the hybrid model of Marthe and Mitra[18], as modified in our previous work on Mn^{III}(salicylate) chains.[4] The expression for the magnetic susceptibility becomes:

$$\chi_{M\prime} = \chi_M/(1 - 2zJ'\chi_M/Ng^2\mu_B{}^2)$$

The best fit parameters obtained are $J = -0.18$ cm^{-1}, $D = -7.85$ cm^{-1}, and $zJ' = 0$ cm^{-1} with $g_{\parallel} = 1.99$ and $g_{\perp} = 1.98$. The best fits calculated for both χ vs T and μ vs T are illustrated in Figure 9.

Magnetic susceptibility of [(NH$_4$)$_2$[Mn^{III}(malonate)$_2$(CH$_3$OH)$_2$][Mn^{III}(malonate)$_2$]]$_n$ (2). The temperature-dependent magnetic susceptibility of [(NH$_4$)$_2$[Mn^{III}(malonate)$_2$(CH$_3$OH)$_2$]-[Mn^{III}(malonate)$_2$]]$_n$ in a magnetic field of 10 kOe is shown in Figure 10. Isothermal magnetization data as a function of field strength were obtained between 50 and 15 kOe at 4.17 K. Since the susceptibility does not turn over at the lowest temperatures studied, it is assumed that the intrachain interactions are small and that the chain may also be treated by the hybrid model of Marathe and Mitra,[18] as modified in our previous work on Mn^{III}-(salicylate) chains. The best fit parameters obtained are $J = 0.09$ cm^{-1}, $D = -7.6$ cm^{-1}, and $zJ' = 0$ cm^{-1} with $g_{\parallel} = 2.09$ and $g_{\perp} = 2.03$. The best fits calculated for both χ vs T and μ vs T are illustrated in Figure 10.

Magnetic susceptibility of [Na$_2$[Mn^{III}(malonate)$_2$][Mn^{III}-(malonate)$_2$(CH$_3$OH)]·(CH$_3$OH)]$_n$ (3). The temperature-dependent magnetic susceptibility of [Na$_2$[Mn^{III}(malonate)$_2$][Mn^{III}(malonate)$_2$(CH$_3$OH)]·(CH$_3$OH)]$_n$ in a magnetic field of 10 kOe is shown in Figure 11. Isothermal magnetization data as a function of field strength were obtained between 50 and 15 kOe at 4.17 K and behavior similar to that of the potassium and ammonium compounds was observed.

As noted above, **3** (the Na$^+$ salt), has a complex three-dimensional structure with several pathways for superexchange between the Mn^{III} $S = 2$ ions, and there is no evidence for long-range ordering. Although one predicts that magnetic exchange through the Mn(1)–Na(1) pathway would be negligible, the interpenetrating manganese chains significantly complicate the interpretation of the magnetism in this system. Rushbrooke and Wood[19] showed that the theoretical curves for magnetic susceptibilities above the critical temperature are rather insensitive to the precise lattice structures. An attempt was made to construct a hybrid model by using the zero field splitting term from Marathe and Mitra[18] and the results for three-dimensional structures given in the work by Lines.[20] The fitting calculations were unsuccessful. For the sake of completeness and since an alternating chain can be identified in the structure, the hybrid chain model were fit to the data, and the resulting spin-Hamiltonian parameters for **3** are $J = -0.24$ cm^{-1}, $D = -7.85$ cm^{-1}, and $zJ' = 0$ with $g_{\parallel} = 1.96$

(18) Marathe, V. R.; Mitra, S. *Chem. Phys. Lett.* **1974**, *27*, 103.

(19) Rushbrooke, G. S.; Wood, P. *J. Mol. Phys.* **1958**, *1*, 257.

(20) Lines, M. E. *J. Phys. Chem. Solids* **1970**, *31*, 101.

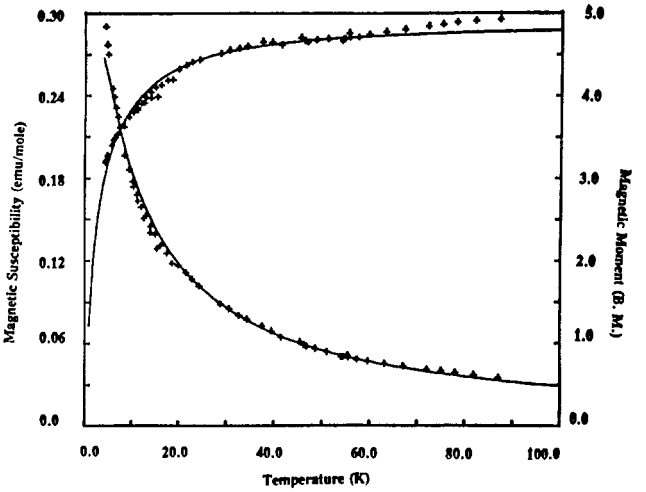

Figure 11. Temperature dependent magnetic susceptibility of **3** in a magnetic field of 10 kOe. The best fit parameters obtained are $J = -0.24$ cm^{-1}, $D = -7.85$ cm^{-1}, and $zJ' = 0$ cm^{-1} with $g_{\parallel} = 1.96$ and $g_{\perp} = 2.02$. The best fits calculated for both χ vs T and μ vs T are illustrated as solid lines.

and $g_{\perp} = 2.02$. The best fits calculated for both χ vs T and μ_{eff} vs T are shown in Figure 11. These results should be viewed with caution in view of the assumptions underlying the model used for the fitting calculations and these parameters do not warrant further discussion.

Discussion

Inspection of the magnetic and structural data for the salicylate and malonate A–B chain compounds reveals that a striking magnetostructural correlation is emerging. Data for the malonate chains **1** and **2** and the salicylate chains **4** and **5** may be compared. Interestingly, $[(NH_4)_2[Mn^{III}(salicylate)_2][Mn^{III}(salicylate)_2(CH_3OH)_2]]_n$ (**6**) shows the onset of long-range ordering while the $[(NH_4)_2[Mn^{III}(malonate)_2][Mn^{III}(malonate)_2(CH_3OH)_2]]_n$ chain does not. The malonate chain **3** has a markedly different structure type than the other solids described herein. The spin-Hamiltonian parameters for **3** and **6** reflect these added complications.

It was of particular interest to compare the malonate and salicylate systems since the donor capacities and charge transfer tendencies of the two ligand types are markedly different. Despite the very different pK_a values of phenolate and carboxylate oxygen atoms, the angles and bond distances in the superexchange pathways for the four compounds **1**, **2**, **4**, and **5** are very similar. It is reassuring to note that the spin-Hamiltonian parameters, summarized in Table VI, are also very similar. The consistency of the data leads some credence to the hybrid model that has been used to analyze the magnetic data. However, a direct measurement of the spin-Hamiltonian parameter D would have a marked influence on the understanding of the exchange and zero field splittings in these compounds. These results stimulate additional efforts to produce Mn^{III} ($S = 2$) A–B chains which have a greater variation in metric parameters through chemically more drastic changes to the ligand set.

Table VI. Magnetic Parameters for Malonate and Salicylate Chains

chain	$g_{\parallel}$	$g_{\perp}$	J, cm^{-1}	D, cm^{-1}	Zj', cm^{-1}
1	1.99	1.98	−0.18	−7.9	0.0
2	2.09	2.03	−0.09	−7.6	0.0
3[a]	**1.96**[b]	**2.02**	**−0.24**	**−7.85**	0.0
4	2.00	2.00	−0.23	−9.0	0.0
5	2.09	2.03	−0.70	−7.0	0.0
6	2.00	2.00	−0.23	−20.3	−0.81

[a] This compound forms a three-dimensional lattice. [b] Values in bold face were from the best fit parameters using a model for simple AB chains.

Acknowledgment. The authors acknowledge many useful conversations on this topic with Dr. Martin L. Kirk. This work was supported by NIH (Grant No. 38409 to VLP) and NSF (Grant No. CHE-9111-08 to WEH). V.L.P. also wishes to thank the Alfred P. Sloan Foundation for a Fellowship and the Department of Chemistry, University of North Carolina, Chapel Hill, NC, for an appointment as a visiting professor.

Supplementary Material Available: Tables providing a full crystallographic summary for **2** and **3** provide anisotropic thermal parameters of all non-hydrogen atoms, fractional atomic positions for hydrogen atoms, a complete set of bond distances, and a complete set of bond angles and figures providing plots of magnetic susceptibility and effective magnetic moments, magnetization vs applied field, and complete numbering schemes for all atoms for **2** and **3** (14 pages). Ordering information is given on any current masthead page.